Core tungsten transport in long pulse WEST L-mode plasmas

X. Yang[1, 5], P. Manas[2], C. Bourdelle[2], JF. Artaud[2], Y. Camenen[3], C. Desgranges[2], P. Devynck[2], T. Dittmar[4], A. Ekedahl[2], N. Fedorczak[2], O. Meyer[2], J. Morales[2], T. Loarer[2], G. Urbanczyk[2], D. Vézinet[2], L. Zhang[5], X. Gong[5]

[1]*University of Science and Technology of China, Hefei, People's Republic of China*

[2]*CEA, IRFM, F-13108 Saint Paul-Lez-Durance, France.*

[3]*CNRS, Aix-Marseille Univ., PIIM UMR7345, Marseille, France*

[4]*Forschungszentrum Jülich GmbH, Institut für Energie- und Klimaforschung—Plasmaphysik, D-52425 Jülich, Germany*

[5]*Institute of Plasma Physics, Chinese Academy of Sciences, Hefei, People's Republic of China*

Tungsten (W) accumulation in the core of tokamak plasmas can cause large increase of the radiated power due to its high cooling rate, which could severely restrict the operational domain. Indeed, it is routinely observed in machines with tungsten environments such as JET and ASDEX Upgrade, that W accumulates in particular conditions, e.g. in high NBI heated H-mode plasmas. In this context, the tokamak WEST, which operates in a full W environment, has achieved 32s L-mode pulses without any sign of W accumulation. Therefore, it is important to understand tungsten transport in these low torque, RF dominant electron heated WEST pulses, for future optimized operations.

W transport results of both neoclassical (collisional) and turbulent physics. Neoclassical particle convection, is proportional to the normalized density and ion temperature gradients [1]. Hence electron density peaking plays a key role in W accumulation. In presence of toroidal rotation, the detrimental effect of density peaking is further amplified [1]. On the other hand, microinstabilities, such as Ion Temperature Gradient (ITG) and Trapped Electron Mode (TEM) driven turbulence, are predicted to also produce significant impurity transport in these L-mode plasmas from r/a=0.3-1. Thanks to the neoclassical code NEO [2] and the quasi-linear gyrokinetic code Qualikiz [3-5], W transport analysis can be tackled. In this contribution, a description is given of one of the WEST long pulse L mode plasmas, where despite peaked electron densities, the W concentration remains stable throughout the whole pulse.

1. Experimental observations

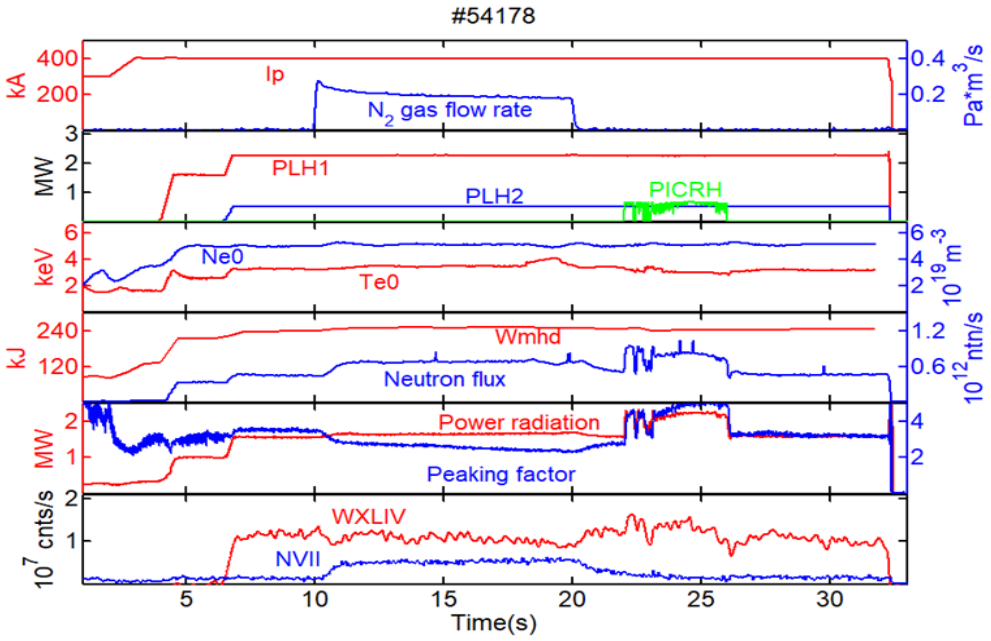

Figure 1. Time Traces of (a) plasma current and the N_2 puff flow rate from the upper divertor, (b) heating powers, (c) central Te and Ne, (d) plasma stored energy Wmhd and the neutron flux, (e) total power radiation and peaking factor defined as $(I_{23}/Ne(0)/L_{23})/(I_{16}/Ne(0.4)/L_{16})$, with I line integrated SXR intensity and L the length LOS of SXR., (f) line emissions of WXLIV and NVII.

In the C3 campaign, WEST has achieved up to 37s L-mode pulses. Time traces of some parameters of one representative WEST long pulse (toroidal magnetic field B_T=3.7T) plasma are presented in Figure 1. This pulse was performed in upper single null and N_2 was seeded to study ammonia formation [6]. Throughout the discharge heated via Lower Hybrid Current Drive (LHCD) antennas with up to 2.8 MW, the radiated power, the peaking factor (defined as ratios of SXR line integrated intensities) and the UV line emission of WXLIV display a stable behavior which suggests that the W content remains stable, showing no sign of accumulation. Increased radiated power is only observed during the Ion Cyclotron Resonance Heating (ICRH) phase and is not further discussed in this paper, more details on the plasma response in presence of ICRH are reported in [7]. Additionally, it is to be noted that during N_2 seeding, the plasma stored energy and the neutron flux increase, indicating increased confinement.

2. Theoretical modelling

Regarding W transport, the stationary phase at 8s, prior to N_2 seeding, has been scrutinized with the transport codes Qualikiz and NEO at r/a=0.5 first. Input data were extracted from interferometry inversion / reflectometry (electron density profiles, figure 2.a), electron cyclotron emission (electron temperature profiles). Other quantities such as the effective

charge Z_{eff}, the N and W content, the ion temperature profiles were reconstructed with the integrated modelling suite METIS [8]. Based on resistive Z_{eff} estimates in the diverted ohmic phase and on the core radiated power, N, Cu and W concentrations are included at the following levels 2%, $7.5*10^{-4}$, and $2.6*10^{-4}$ respectively. The central ion temperature is scaled to match the neutron flux, yielding ratios of T_e/T_i at mid-radius of the order of 1.8. Finally, the electron and ion heat fluxes are computed in METIS, taking into account the power deposition from LHCD, the collisional equipartition and the radiated power. Important parameters for the following analysis are gathered in Table 1.

r/a	R/L_{Te}	T_e/T_i	s	q	Z_{eff}	ν^*	Q_e METIS kW/m²	Q_i METIS kW/m²
0.5	15	1.8	0.9	1.7	2.8	0.5	46	15

Table 1. Plasma parameters used in NEO and QuaLiKiz simulations

2.1 Mid-radius electron density peaking

Due to large uncertainties in the above derived quantities such as the ion temperature profiles, a scan in the normalized gradients R/L_{Ti} and R/L_n, which drive ITG and TEM turbulence respectively, has been performed. The stable/TEM/ITG domains are shown in Fig 2(b) together with the heat fluxes matched and the zero particle flux conditions, the latter being determined by the compensation of the Ware pinch and the turbulent flux.

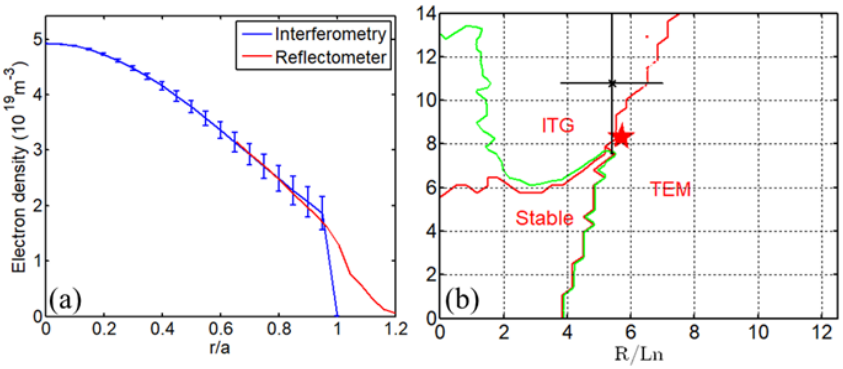

Figure 2. (a) Electron density profile at 8s. (b) Stability analysis (QuaLiKiz) versus R/L_{Ti} and R/L_{ne}. The estimated gradient values are shown in black with their error bars. The matched heat fluxes condition is represented by the red star. The green line, i.e. the balance of the Ware pinch ($7.10^{17}m^{-2}s^{-1}$) and of the turbulent particle flux, gives the zero particle flux condition.

It is found that the heat flux matched condition is met in the TEM domain which is due to the dominant electron heating (Q_e/Q_i = 3), and close to the ITG and stable regions. Additionally, the zero particle flux condition in this region is limited by the critical density gradient

threshold in quantitative agreement with measured density peaking. In contrast in the ITG domain, this condition is given by the competition between convective and diffusive transport [9] resulting in much lower predicted density peaking ($R/L_n < 2$).

2.2 W density peaking profiles

W density peaking is now scrutinized, including neoclassical transport. To put in perspective with NBI heated plasmas, additional simulations have been performed with an artificially increased toroidal rotation up to 100km/s (corresponds to a Mach number of M=0.36).

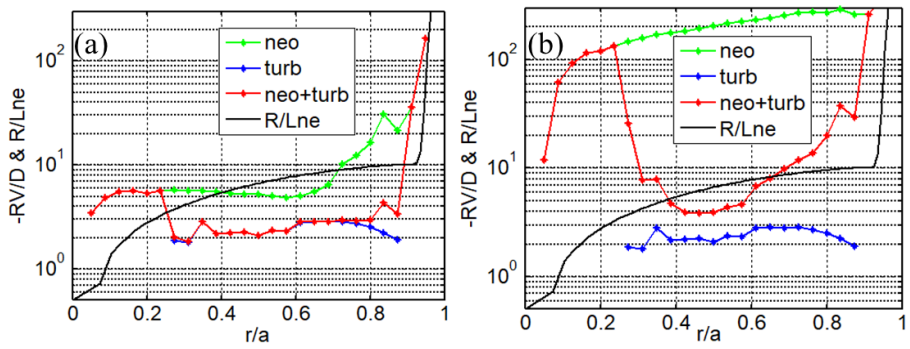

Figure 3. Radial profiles of –RV/D (a) V_{tor}=0 and (b) $V_{tor}(0)$=100km/s. R/L_{ne} is also plotted.

In Figure 3(a), the W peaking is compared to the electron peaking across the whole radial domain. It is found that turbulence flattens the unfavorable neoclassical peaking in most radii except in the inner region (r/a<0.25) where neoclassical transport dominates. Even in the latter region the W density peaking remains modest. This is due to the absence of strong torque and subsequent toroidal rotation in these WEST plasmas. To illustrate this, in Fig 3 (b), the amplified neoclassical transport due to an artificially increased toroidal rotation results in increased W peaking, in particular in the stable region (r/a<0.25) where a factor 20 is found compared to the nominal case without toroidal rotation. This modelling work will be completed by fast flux driven simulation using the integrated platform RAPTOR coupled to a Neural Network version of QuaLiKiz [10,11]. W radiation, neoclassical transport and interplay with MHD will be added. To prepare WEST phase 2, aiming at 1000s H mode [12], this approach will be used in a systematic manner to optimize the scenario design and to prepare real-time control.

[1] C. Angioni, P. Helander PPF 2014 [2] E. Belli et al PPCF (2008) [3]www.qualikiz.com [4] C. Bourdelle et al PPCF (2016) [5] J. Citrin et al PPCF (2017) [6] A. Drenik et al EPS 2019 I2.103 [7] L. Colas et al RFPPC (2019) [8] JF Artaud NF (2018) [9] C. Angioni PPCF 2009 [10] F. Felici et al NF 2018 [11] K. Van De Plassche EPS 2019 P1.1089 [12] C. Bourdelle et al, NF (2015)